Chemistry Europe
European Chemical Societies Publishing

WILEY VCH

Excellence in Chemistry Research

Announcing our new flagship journal

- Gold Open Access
- Publishing charges waived
- Preprints welcome
- Edited by active scientists

Meet the Editors of *ChemistryEurope*

Luisa De Cola
Università degli Studi di Milano Statale, Italy

Ive Hermans
University of Wisconsin-Madison, USA

Ken Tanaka
Tokyo Institute of Technology, Japan

ChemistrySelect

Research Article
doi.org/10.1002/slct.202300404

Chemistry Europe
European Chemical Societies Publishing

www.chemistryselect.org

Natural Molecule-Incorporated Magnetic Organic-Inorganic Nanoflower: Investigation of Its Dual Fenton Reaction-Dependent Enzyme-Like Catalytic Activities with Cyclic Use

Seyma Dadi,[a, b] Marlon Henrique Cardoso,[c, d] Amit Kumar Mandal,[e, f] Octávio Luiz Franco,[c, d] Nilay Ildiz,[g] and Ismail Ocsoy*[a]

The functional organic-inorganic hybrid nanoflowers (hNFs) have recently attracted considerable attention due to enhanced catalytic activity and stability. The main purpose of this study is to synthesize new Fenton reagents and investigate their catalytic activity, dye degradation performance and antimicrobial activity. This magnetic gallic acid nanoflowers (FeGANF) were self-assembled via incorporating magnetic nanoparticles (Fe_3O_4 NPs) into gallic acid (GA) as organic part and copper(II) phosphate ($Cu_3(PO_4)_2$) as inorganic parts. The FeGANF were characterized by SEM, EDX, FT-IR and XRD. The peroxidase-like activity and dye degradation performance of FeGANF and GANF based on Fenton reaction in the presence of H_2O_2 was studied toward guaiacol as substrate, using methylene blue (MB) and congo red (CR) as a cationic and anionic dyes, respectively. FeGANF shows much high catalytic activity and decoloration efficiency (97% for MB and 99% for CR) because of dual active center in Fenton reaction on the surface of FeGANF. FeGANF exhibited more antimicrobial activity against *Escherichia coli* ATCC 25922, *Staphylococcus aureus* ATCC 25923, and *Candida albicans* ATCC 10231 than that of the GA and GANF. The results of these studies suggest that magnetic hNFs has proved to be promising Fenton reagents for biological and environmental applications including treatment of wastewater.

[a] *S. Dadi, I. Ocsoy*
Department of Analytical Chemistry
Faculty of Pharmacy
Erciyes University
38039, Kayseri, Turkey
E-mail: ismailocsoy@erciyes.edu.tr
[b] *S. Dadi*
Department of Nanotechnology Engineering
Abdullah Gül University
38080, Kayseri, Turkey
[c] *M. H. Cardoso, O. L. Franco*
S-inova Biotech
Programa de Pós-Graduação em Biotecnologia
Universidade Católica
Dom Bosco Avenida Tamandaré 6000,
Campo Grande MS, 79117900, Brazil
[d] *M. H. Cardoso, O. L. Franco*
Centro de Análises Proteômicas e Bioquímicas
Pós-Graduação em Ciências Genômicas e Biotecnologia
Universidade Católica de Brasília
SGAN 916 Módulo B, Asa Norte
Brasília DF, 70790160, Brazil
[e] *A. K. Mandal*
Chemical Biology Laboratory
Department of Sericulture
Raiganj University
North Dinajpur, West Bengal 733134, India
[f] *A. K. Mandal*
Centre for Nanotechnology Sciences (CeNS)
Raiganj University
North Dinajpur, West Bengal 733134, India
[g] *N. Ildiz*
Department of Pharmaceutical Microbiology
Faculty of Pharmacy
Erciyes University
38039, Kayseri, Turkey

Supporting information for this article is available on the WWW under https://doi.org/10.1002/slct.202300404

Introduction

Organic-inorganic hybrid material with specific physical and chemical properties has drawn attention to scientists because of having large specific surface area, excellent stability, and catalytic activity, along with a strong adsorption capability.[1] Organic-inorganic hybrid nanoflowers (hNFs) are a class of organic-inorganic hybrid materials. hNFs discovered by Ge *et al.*,[2] are prepared by self-assembled from metal ions as inorganic components, and enzyme or protein as organic component. While enzyme-based hNFs have been produced and used in many potential applications, different studies demonstrate the synthesis of hNFs from non-protein molecules including amino acids, catecholamine and plant functional groups[3–5] in organic molecules create complexes via coordination interactions with metal ions, especially Cu^{2+} ions in phosphate-buffered saline (PBS) to form hNFs.

The high surface-to-volume ratio, excellent stability and enhanced catalytic activity of hNFs have given them a wide range of applications in many fields, including biological sensing,[6] biomimetic catalyst[7] and water treatment.[8] For instance, Lin *et al.*,[9] reported the synthesis of HRP-inorganic hybrid nanoflowers to detect H_2O_2 in spiked serum and phenol in sewage. Additionally, Altinkaynak *et al.*,[10] synthesized hybrid Turkish black radish peroxidase-Cu^{2+} nanoflowers for Victoria blue dye decoloration, having enhanced efficiency compared with free Turkish black radish peroxidase.

The rapid economic development in recent years has led to an increase in serious water pollution.[11] One of the most significant causes of water pollution includes the excessive use of synthetic dyes, including rhodamine B (rhB), congo red (CR), malachite green (MG) and methylene blue (MB).[12] Different

types of dyes are widely used in several industries, including textile, paper, plastic, and rubber. Every year an incredible amount of dye wastewater is directly discharged to rivers and lakes without pretreatment, leading to impairment of water quality and food chain contamination.[13] Moreover, dye wastewater inhibits the photosynthesis capacity of aquatic organisms by reducing the penetration of light to water. Recently, because of increasing awareness of public health and environmental protection, different physical and chemical methods such as physical adsorption and photocatalytic degradation have been developed to deal with dye wastewater.[14] In this context, the Fenton reaction represents an advanced oxidation process for the efficient degradation of dye wastewater. In a Fenton reaction, hydroxyl radicals produced by catalyst attack organic dye compounds, causing the formation of intermediate species, further to CO_2 and H_2O.[15]

Many literature reports have focused on the use of the Fenton process for decolorization and have suggested that $Cu_3(PO_4)_2$-NFs as Fenton reagent can be used in dye decolorization.[10] Therefore, it is imperative to develop a new Fenton reagent based on hNFs with high catalytic activity and removal efficiency for wastewater treatment. Thus, the successful incorporation of Fenton catalysts such as Fe_3O_4 NPs into hNFs can lead to increased catalytic activity and dye removal efficiency.

Previous studies have shown that Fe_3O_4 NPs have been used to mimic the activity of peroxidase enzymes.[17,18] For this reason, we employed Fe_3O_4 NPs as Fenton reagent into hNFs to improve catalytic activity and dye removal efficiency of hNFs. The novelty of this research is 1) for the first time, synthesis of magnetic gallic acid nanoflowers, 2) characterization of magnetic GANF, 3) improvement in catalytic activity and dye removal performance of magnetic GANF with increased Fe_3O_4 NPs concentrations, 4) high antimicrobial activity of magnetic GANF against bacteria and fungi 5) good reusability performance of magnetic GANF.

Results and discussion

Synthesis of hybrid nanoflowers

In nanoflower synthesis, carboxyl groups in gallic acid reacted with Cu^{2+} ions to initiate the nucleation of GA-$Cu_3(PO_4)_2$ primary crystals as seed. In the growth step, the primary nanocrystals continued to react with gallic acid to form large petals, then gallic acid in petals as adhesive molecules bound to each other. In the last step, the synthesis of nanoflower was completed with a saturation of anisotropic.

To efficiently incorporate amino-functionalized Fe_3O_4 NPs to GANF, Fe_3O_4 NPs were vigorously shaken with gallic acid for 1 h followed by adding to PBS at pH 7.4. Then $CuSO_4$ solution was added and incubated for three days. Finally, full blooming of nanoflowers was formed through self-assembly of Fe_3O_4 NPs with gallic acid and Cu^{2+} ions in the PBS. Fe_3O_4 NPs were adsorbed on the petals of GANF through electrostatic attraction.

Characterization of hNFs

The structure of synthesized Fe_3O_4 NPs was characterized via STEM, DLS and zeta potential. In Figure 1A and 1B, STEM images showed that amino-functionalized Fe_3O_4 NPs have spherical shapes with a diameter of ~10 nm in size. The hydrodynamic diameter of the Fe_3O_4 NPs was determined as ~50 nm by DLS (Figure 1C). The NPs are uniform in morphology and have narrow size distribution. The surface charge of the NPs was determined by zeta potential measurement. The NPs had a positive zeta potential value of +15.4 mV in PBS due to the presence of amine groups as ligands (Figure 1D).

Figure 2 showed SEM images of GANF and FeGANF. GANF are spherical in shape and flower-like structures with a diameter of 5 μm, which present a high surface-to-volume ratio and adequate mono-dispersity in Figure 2A and 2B. Figure 2C–2E displays the modified GANF with Fe_3O_4 NPs. As shown in Figure 2, the morphology and the structure of GANF have not changed by modifying Fe_3O_4 NPs. The magnification of SEM image of FeGANF showed that how the NPs attached to the petal surface of hNFs. The reason for attaching NPs to the surface of hNFs is that the positive surface charge of Fe_3O_4 NPs is suitable for interaction between phosphate groups of negative charged $Cu_3(PO_4)_2$.

The EDX spectrum and elemental mapping in Figure 3A and 3B display element presence and distribution of FeGANF. Elemental mapping of FeGANF provides information about Fe_3O_4 NPs adsorbed to the surface of GANF, where representative element corresponding to $Cu_3(PO_4)_2$ (Cu, P and O) and NPs (Fe). These results show that Fe_3O_4 NPs adsorb to the surface of GANF.

The chemical structure of Fe_3O_4 NPs, GANF and FeGANF were evaluated by FT-IR, as shown in Figure 3C. In the FT-IR spectra of FeGANF, the characteristic peaks of Fe_3O_4 NPs and GANF were observed. Compared with GANF, the new absorption peaks at 2892 cm^{-1} and 2988 cm^{-1} for FeGANF can be ascribed to the N–H stretching vibrations of 1,6 hexanediamine at Fe_3O_4 NPs and asymmetric or symmetric stretching vibrations of aliphatic groups of Fe_3O_4 NPs.[19] The peaks at 1355 cm^{-1} for Fe_3O_4 NPs and 1393 cm^{-1} for FeGANF are derived from the –C–N– stretching of 1,6 hexanediamine at Fe_3O_4 NPs.[20] GANF and FeGANF showed the same absorption band at 1038 cm^{-1}, 1042 cm^{-1} and 558 cm^{-1} which are assigned to P–O vibrations of $Cu_3(PO_4)_2$.[21] Accordingly, FT-IR results demonstrated that Fe_3O_4 NPs was successfully introduced into FeGANF.

The structure and phase analysis of Fe_3O_4 NPs, GANF and FeGANF was employed by X-ray diffraction (XRD). As shown in Figure 3D, the crystalline diffraction peaks at 30.17°, 35.62°, 57.22° and 62.38° correspond to (220), (311), (551) and (440) diffraction planes of Fe_3O_4 NPs which are matced with Fe_3O_4 NPs.[22–24] Both GANF and FeGANF display diffraction peaks similar to standard cards (JCPDS#22-0548), indicating the main constituent of samples was $Cu_3(PO_4)_2$.[21,25] Moreover, FeGANF exhibits a diffraction peak at 35.57°, corresponding to the (311) plane of Fe_3O_4 NPs. According to these results, the crystal structure of FeGANF did not change and Fe_3O_4 NPs was successfully incorporated into FeGANF.

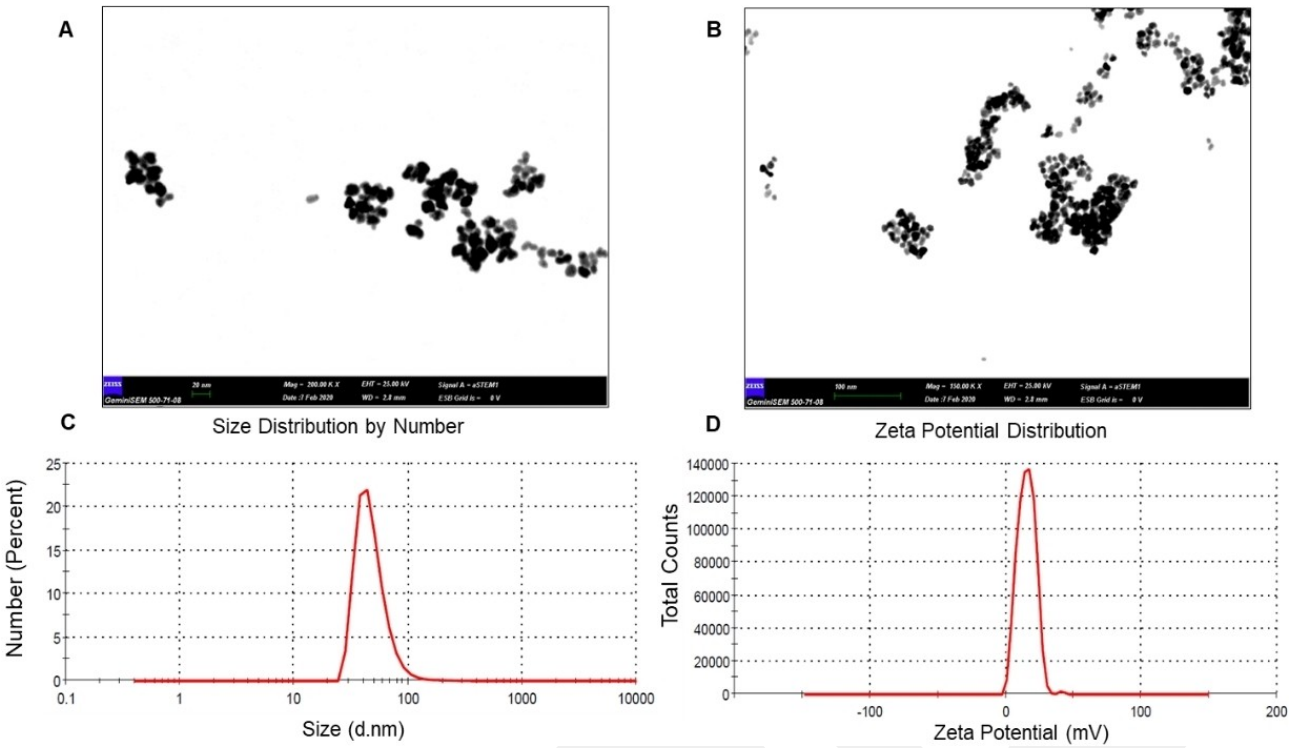

Figure 1. (A and B) STEM image of Fe_3O_4 NPs, (C) DLS data of Fe_3O_4 NPs, (D) Zeta potential of Fe_3O_4 NPs.

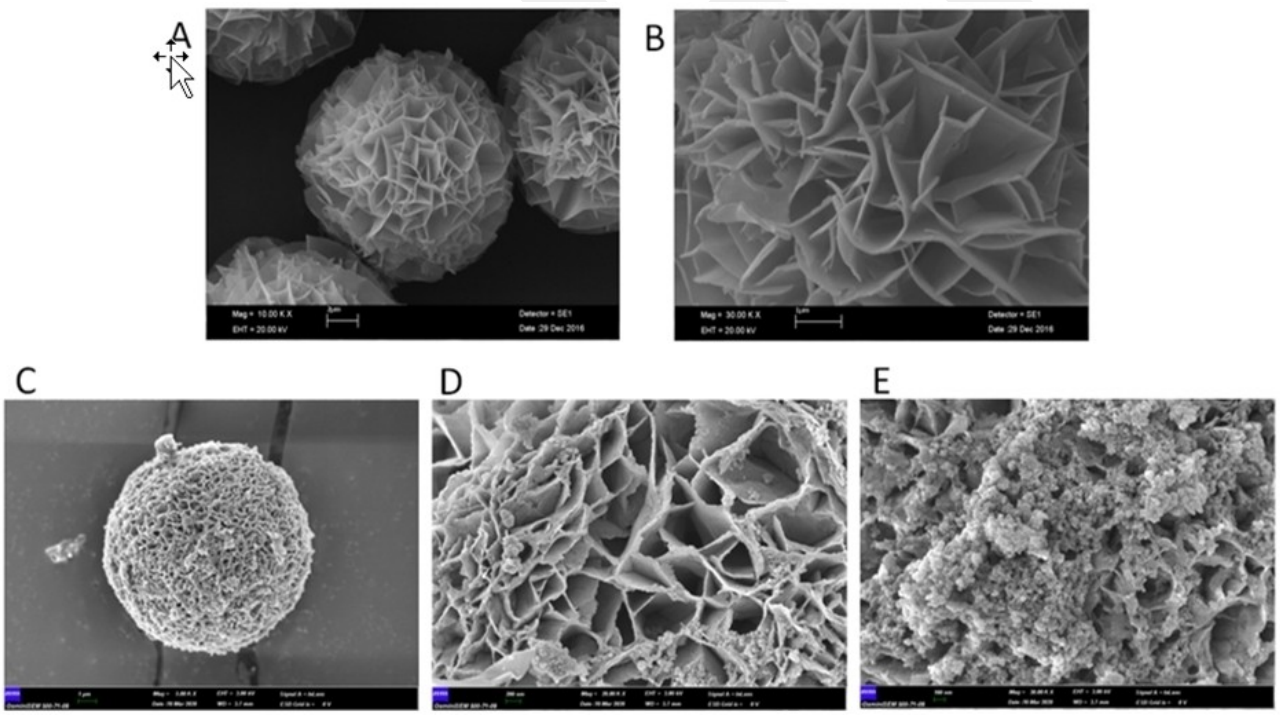

Figure 2. (A) SEM image of GANF, (B) SEM image of magnified GANF with boundaries. (C) SEM image of FeGANF, (D and E) SEM image of magnified FeGANF with different 10 mg and 20 mg Fe_3O_4 NPs, respectively.

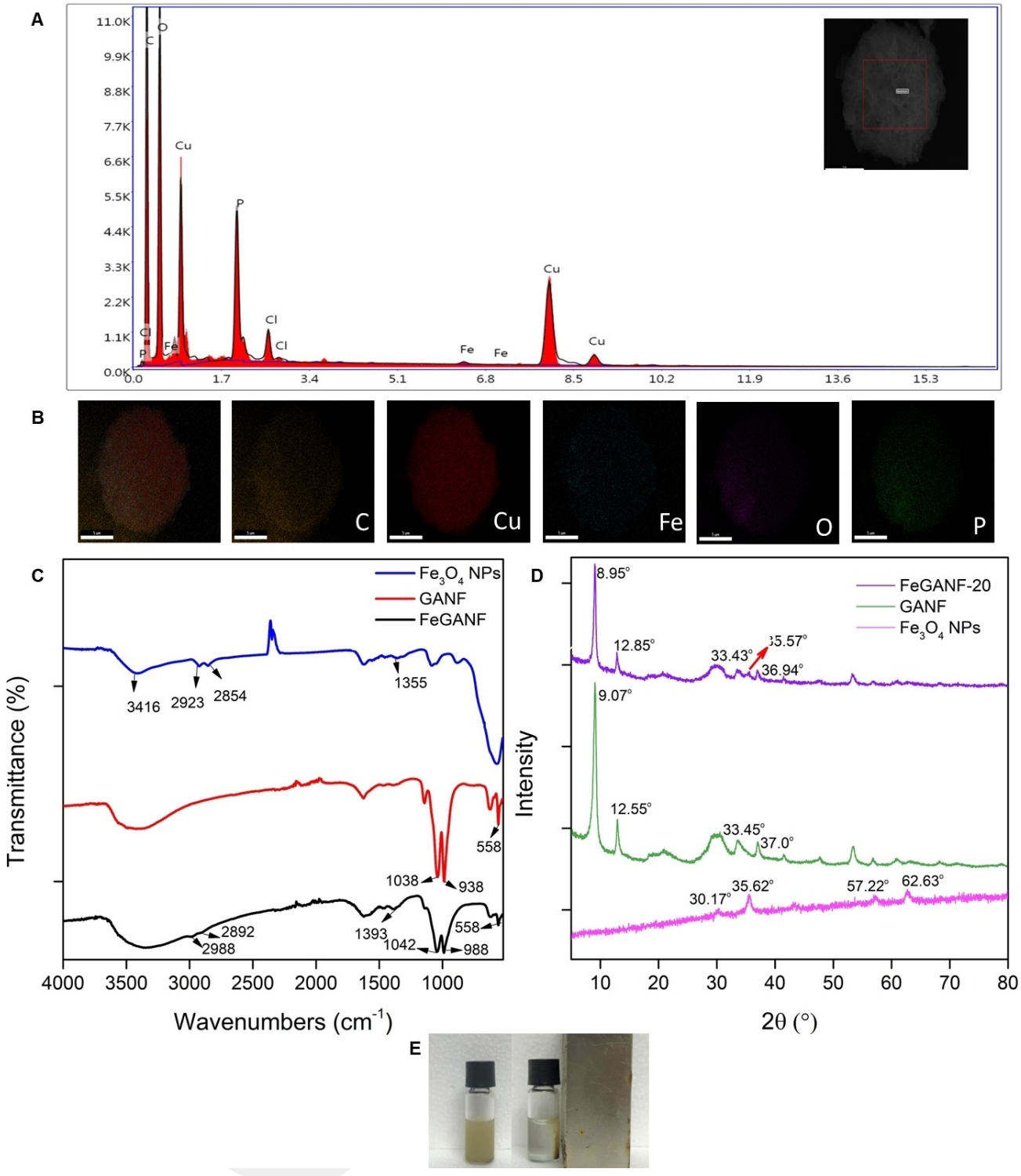

Figure 3. (A) EDX spectrum of FeGANF. Figure inset showing SEM micrograph of FeGANF (B) Elemental mapping of FeGANF. (C) FT-IR spectrum of Fe_3O_4 NPs, GANF and FeGANF (D) XRD spectrum of Fe_3O_4 NPs, GANF and FeGANF (E) Magnetic separation of FeGANF from solution.

Peroxidase-like activity of hNFs

Peroxidase-like activity of hNFs was investigated by using guaiacol (GA) as the model substrate. hNFs can catalyze the oxidation of colorless GA into amber-colored 3′-dimethoxy-4,4′-biphenylquinone in the presence of H_2O_2, with a new absorption peak emerged at 470 nm observed in the UV-Vis spectra. Peroxidase-like activity of hNFs depends on a Fenton-like mechanism. The potential mechanism for the Fenton-like reaction of the hNFs is shown in Eq. 1.[26]

$$Cu^{2+} + H_2O_2 \rightarrow Cu^{+} + HOO^{\cdot} + H^{+}$$
$$Cu^{+} + H_2O_2 \rightarrow Cu^{2+} + OH^{\cdot} + OH^{-}$$
$$Fe^{2+} + H_2O_2 \rightarrow Fe^{3+} + OH^{\cdot} + OH^{-} \quad (1)$$
$$Fe^{3+} + H_2O_2 \rightarrow Fe^{2+} + HOO^{\cdot} + H^{+}$$

As shown in Eq. 1 the hydroxyl radicals (•OH) are the main reactive species in the Fenton processes. Cu^{2+} ions in hNFs react with H_2O_2 to form Cu^{+} ions and then •OH are formed as a result of the reaction of Cu^{+} with H_2O_2. Additionally, Fe^{2+} reacts with H_2O_2 to generate Fe^{3+} and •OH and, subsequently, Fe^{3+} ions are reduced to Fe^{2+}.

According to Eq. 1, catalytic activity is determined by the •OH originated from hNFs catalyzed H_2O_2 decomposition. The amount of •OH depends on the composition of hNFs and H_2O_2 concentration. In this study, the effect of H_2O_2 concentration, the amount of Fe_3O_4 NPs in GANF and pH of reaction condition was studied to investigate the catalytic activities of hNFs.

The catalytic activities of GANF and FeGANF-10 (10 mg Fe_3O_4 NPs in GANF) are close to each other as the concentration of H_2O_2 increases. In the presence of 22.5 mmol L^{-1} H_2O_2, FeGANF-20 (20 mg Fe_3O_4 NPs in GANF) having more Fe_3O_4 NPs shows significant catalytic activity compared to GANF and FeGANF-10 (Figure 4A). The enhancement in the catalytic activity of FeGANF-20 is due to the formation of more •OH as a result of the dual Fenton reaction. The catalytic activity of hNFs is closely associated with the pH value of the reaction solution. To find proper pH value for the Fenton like reaction, experiments were applied at different pH values (pH 4, pH 7, and pH 10). As shown in Figure 4B, the maximum catalytic activity was observed at pH 7.

Dye degradation performance of hNFs

Wastewater from leather, paper and plastic contains organic dyes harmful to human health and the environment.[13] Therefore, wastewater must be pre-treated before being discharged. Recently, various water remediation systems have been developed for the treatment of wastewater. Photo-degradation is widely used due to its cost-effectiveness and simplicity. In the photo-degradation process, organic dyes are oxidized to intermediate species and eventually CO_2 and H_2O.[27–29]

In recent years, hNFs have received considerable attention in dye decolorization applications due to having metal cation and porous structure.[10,30] In the present work, the photocatalytic behaviour of synthesized hNFs was evaluated by using CR as anionic dye and MB as a cationic dye. The Fenton reaction using H_2O_2 to generate •OH are used for the degradation of MB and CR. According to Eq. 1, •OH are generated as a result of reaction of Cu^{2+} and Fe^{2+} ions in hNFs with H_2O_2. Highly reactive •OH attack MB and CR and effectively degrade them as less harmful products.[31]

Herein, firstly, the concentration of dye, hNFs and H_2O_2 were fixed at 0.5 mg mL^{-1}, 1.5 mg mL^{-1} and 22.5 mmol L^{-1}, respectively, and the degradation of the dyes was carried out under sunlight. The decrease in the absorption peak at 664 nm for MB and 488 nm for CR as a function of time was used to investigate the photocatalytic activity of the hNFs. From Figure 5A and 6A, it can be seen that, in the presence of FeGANF-20, the intensity of absorption peak at 664 nm for MB and 488 nm for CR decreased with extension of incubation time. As shown in Figure 5B, the degradation of MB with FeGANF-20, FeGANF-10 and GANF reached 97%, 87% and 78%, respectively, after incubation for 120 min.

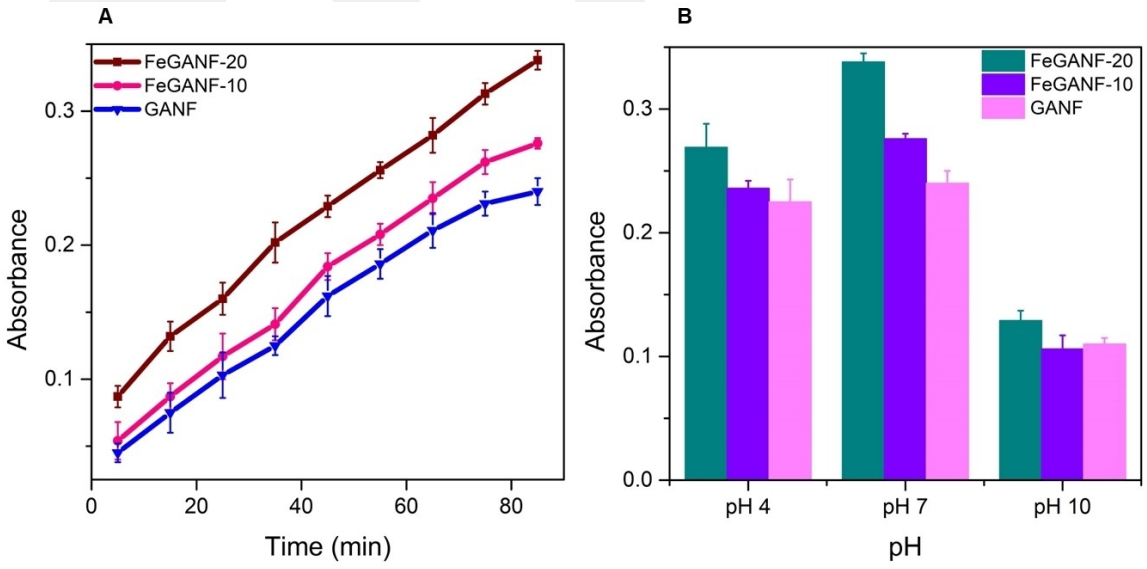

Figure 4. (A) Catalytic activities of hNFs. (B) Effect of pH on the catalytic activity of hNFs.

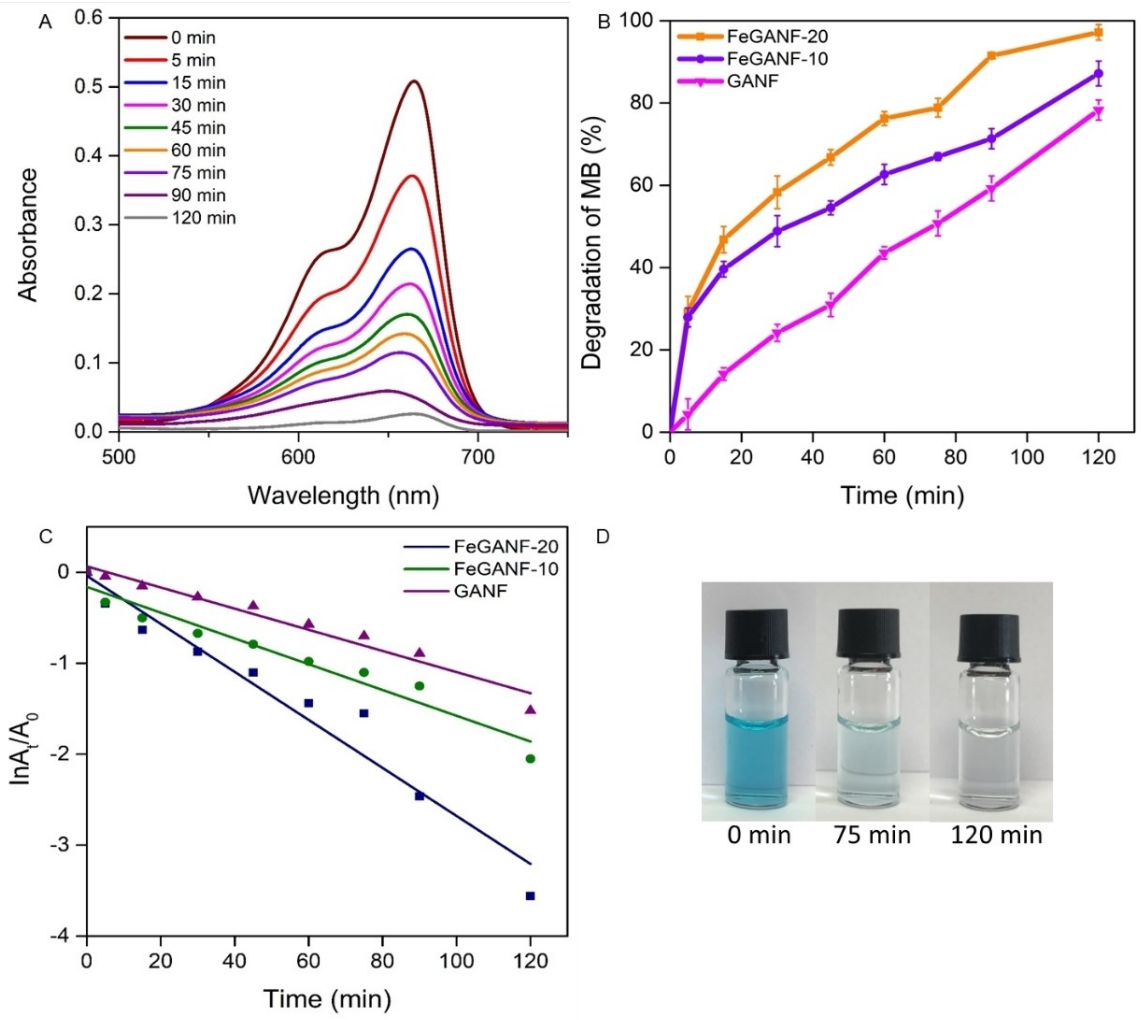

Figure 5. (A) Variation of absorbance spectra of MB in the presence of H_2O_2 by FeGANF-20. (B) Degradation percentage of MB by FeGANF-20, FeGANF−10 and GANF. (C) Kinetics of MB decoloration by FeGANF-20, FeGANF−10 and GANF. (D) Color change of MB solution with time.

The degradation rates of CR were 99%, 93% and 60% for FeGANF-20, FeGANF-10 and GANF, respectively, within 150 min (Figure 6B). Additionally, Figure 5D and 6D show noticeable color change with time. The results reveal that degradation of FeGANF-20 and FeGANF-10 is more efficient than GANF for two dyes. As the amount of Fe_3O_4 NPs in GANF increases, the degradation efficiency of dyes enhances even more. This event explains that abundant Fe_3O_4 NPs accelerate Fe(III)/Fe(II) redox reactions result in a higher ability to generate more •OH that effectively attack the dyes.

In order to investigate the possible mechanism in the present reaction system, isopropyl alcohol (IPA) was selected because it is a scavenger for •OH.Figure S1 demonstrates the role of IPA of different concentrations on the MB degradation process. As IPA reacts with •OH, MB degradation was inhibited. The degradation efficiency of MB was 80% in the presence of 2 mM IPA. However, the degradation of MB dropped to 46% and 15% when 10 mM and 20 mM IPA was added. Based on this result, it is clearly confirmed that •OH play a major role in the MB degradation.

The reaction kinetics is another way to investigate the degradation efficiency of hNFs. Figure 5C and 6C show that a linear relationship exists between ln (A_t/A_0) and time. These results emphasize that the kinetics of hNFs for degradation of MB and CR can be investigated with first-order kinetics models.[4] The first-order kinetic model can be expressed in the following equation in Eq. 2.

$$\ln(C_t/C_0) = \ln(A_t/A_0) = -kt \quad (2)$$

where, C_0 and C_t are the concentration of the dyes at times 0 and t. A_0 and A_t are the absorbance values of the dyes at times 0 and t. k is the first-order rate constant. Rate constant k value indicates the effectiveness of the photocatalyst and it can be determined from the slope of $\ln(A_t/A_0)$ and time.

As depicted in Table 1, FeGANF-20 exhibits a higher rate constant for MB (0.026 min^{-1}) and CR (0.028 min^{-1}). The

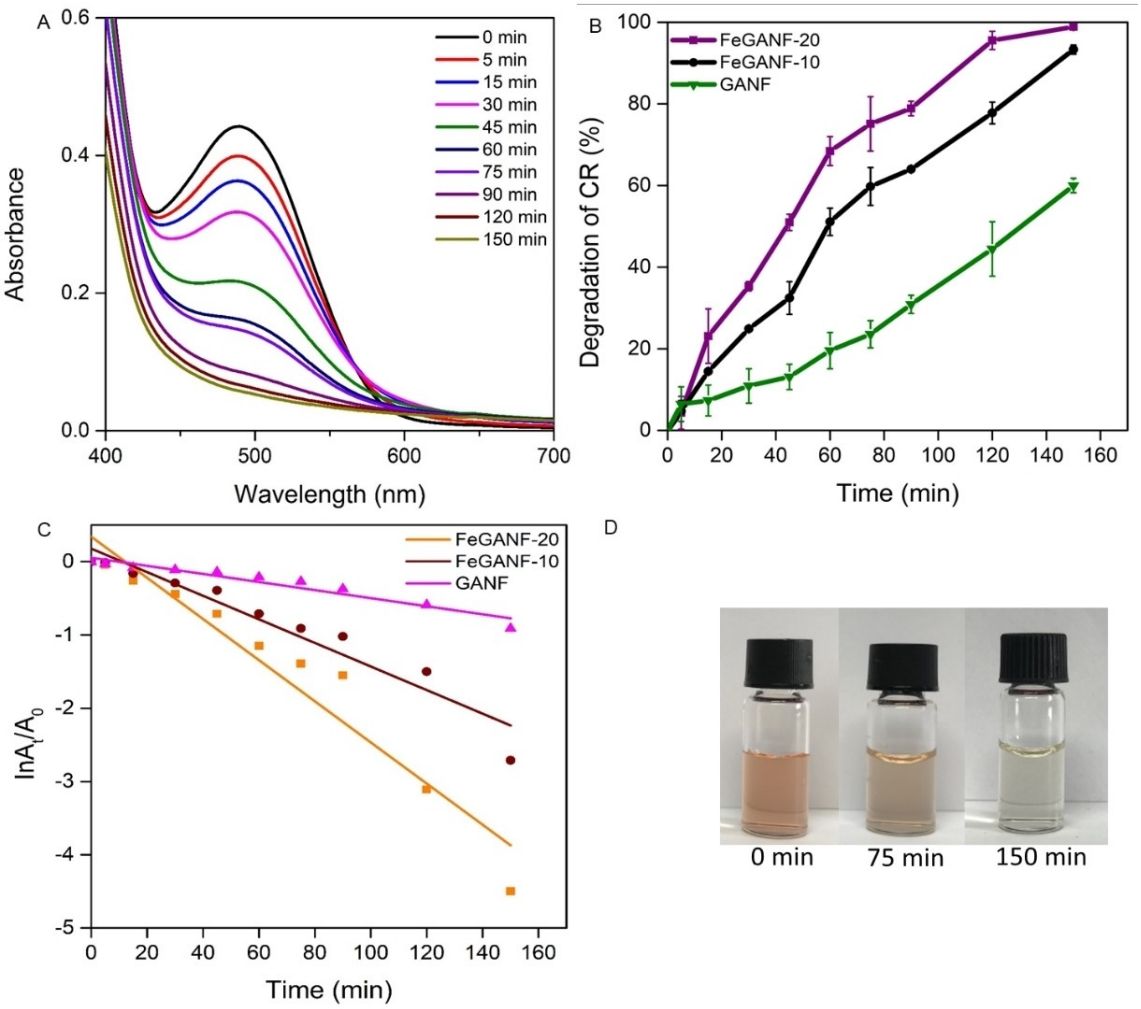

Figure 6. (A) Variation of absorbance spectra of CR in the presence of H2O2 by FeGANF-20. (B) Degradation percentage of CR by FeGANF-20, FeGANF−10 and GANF. (C) Kinetics of CR decoloration by FeGANF-20, FeGANF−10 and GANF. (D) Color change of CR solution with time.

Table 1. Degradation efficiency and kinetic parameters for MB and CR.

hNFs	% degradation of MB	R^2	k	% degradation of CR	R^2	k
FeGANF-20	97 ± 1.9	0.9455	0.02641	99 ± 1	0.92675	0.02808
FeGANF-10	87 ± 3	0.94168	0.01417	93 ± 1.1	0.91984	0.01609
GANF	78 ± 2.5	0.9539	0.01163	60 ± 1.8	0.92585	0.00551

obtained k values increased from 0.0141 to 0.0264 and from 0.016 to 0.028 for MB and CR degradation, respectively when the Fe_3O_4 NPs concentration in GANF increased.

The degradation efficiency of FeGANF-20 is comparable or higher than that of previously reported hNFs or nanozymes (Table 2). FeGANF-20 can be employed as a promising nano-catalyst for the waste-water treatment.

To evaluate the stability and activity of FeGANF-20 upon multiple photo-degradation, an experimental procedure including washing and magnetic separation was applied. FeGANF-20 was easily separated from the solution after each cycle by applying an external magnetic force. For the first eight runs, MB and CR degradation rate indicate a decrease at each cycle, and residual decoloration efficiency at the eighth cycle was 72% for MB and 60% for CR (Figure 7A and 7B). The potential reason is that reduction of dye decoloration efficiency of FeGANF-20 after repeated use can be leaching of Fe from FeGANF-20 during the Fenton process.[37] The other reason can be attributed to the adsorption of dyes and their intermediate species on the active site of FeGANF-20, obstructing the formation of •OH.[38]

Table 2. Comparison of kinetic parameters of FeGANF-20 with other hNFs and nanozymes.

Catalyst	Dye	k (min^{-1})	Time (min)	Degradation efficiency (%)	Reference
Kanamycin-$Cu_3(PO_4)_2$ hybrid flowers	Methylene blue	0.015	240	100	[33]
SC–$Cu_3(PO_4)_2 \cdot 3H_2O$ nanoflowers	Methylene blue	0.014	60	–	[30]
	Rhodamine B	0.0041	60		
	Rhodamine 6G	0.0036	60		
Fe_3O_4 microrods	Rhodamine B	0.038	90	98	
	Methylene blue	0.011	90	77	[34]
	Methyl orange	0.007	90	60	
Co_3O_4-g-C_3N_4	Rhodamine B	0.014	120	100	[35]
Hemin-GDY	Methylene blue	0.0355	120	98.4	[36]
FeGANF-20	Methylene blue	0.026	120	97	This work
	Congo red	0.028	150	99	

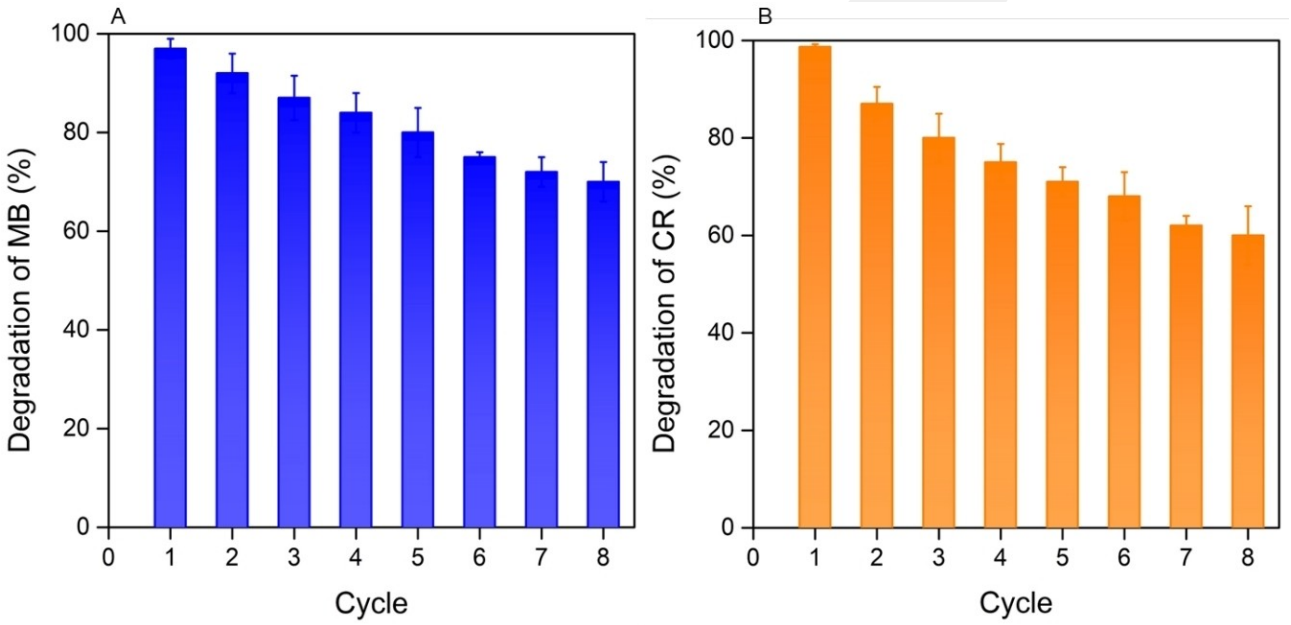

Figure 7. Recyclability of FeGANF-20 for degradation of (A) MB and (B) CR.

Table 3. MIC of GA, GANF and FeGANF-20 against bacteria and fungi.

Material	*E. coli*	*S. aureus*	*C. albicans*
GA	$\geq$1000	1000	1000
GANF	500	500	500
FeGANF-20	500	500	500
GANF 10% H_2O_2	500	50	50
FeGANF-20 10% H_2O_2	50	50	50
GANF 20% H_2O_2	50	50	50
FeGANF-20 20% H_2O_2	50	50	50

Antimicrobial activity

The antimicrobial property of hNFs was tested against *E.coli*, *S. aureus* and *C. albicans*. MIC and inhibition zone values were given at Figure 8 and Table 3. In comparison with the control groups (GA, GANF and FeGANF-20) FeGANF-20 and GANF in the presence of H_2O_2 caused a significant antimicrobial effect, which could potentially be a result of $^{\bullet}OH$ generation from FeGANF-20 and GANF. According to the MIC results, application of 50 μg/mL GANF and FeGANF-20 with H_2O_2 have been reported to have an inhibitory effect against *E. coli*, *S. Aureus* and *C. albicans*. Figure 8 showed that the maximum zone of inhibition was found to be 29.3 ± 0.9, 48.48 ± 0.7 and 54.52 ± 1.1 when used FeGANF-20 in the presence of 20% H_2O_2 against *E. coli*, *S. aureus* and *C. albicans*, respectively. The mechanism of antimicrobial activity of nanomaterials have not been fully

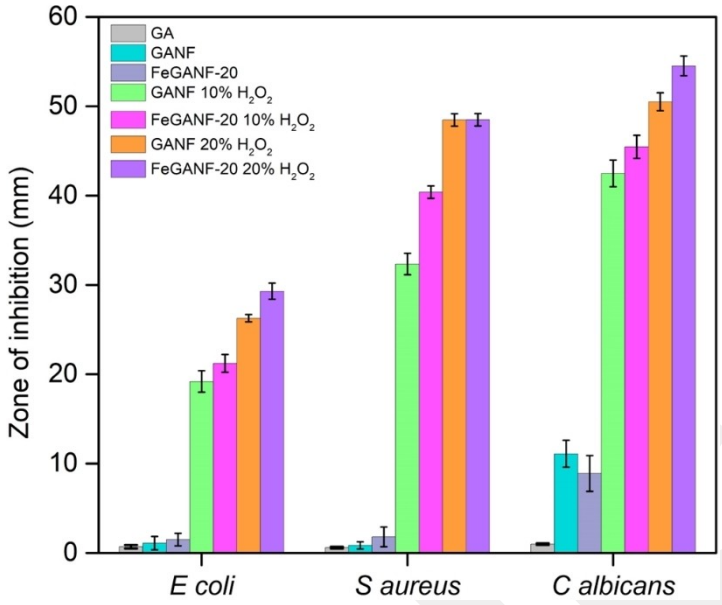

Figure 8. Antimicrobial activities of hNFs.

explained.[39] But our proposed mechanism of antimicrobial activity can be reported as rapid denaturation of cells via •OH induced membrane damage.[40,41]

Conclusion

In conclusion, FeGANF was successfully synthesized by the physical adsorption of Fe_3O_4 NPs on the petal surface of the GANF. Peroxidase-like activities, dye removal performance and antimicrobial activity of synthesized hNFs were investigated under optimal conditions. It was found that Fe_3O_4 NPs in GANF could effectively increase catalytic, dye degradation and antimicrobial activity due to the dual Fenton reaction. Among three synthesized hNFs, the highest peroxidase-like and dye degradation activity toward guaiacol, MB as a cationic dye and CR as anionic dye were accomplished with FeGANF-20. The decoloration efficiency of FeGANF-20 for MB and CR is 97% and 99% within 120 min and 150 min, respectively. The hNFs show excellent antimicrobial activity in the presence of H_2O_2. In summary, this work presents a method for the synthesis of magnetic hNF. This does not only increase the catalytic activity but also provides an optimized separation performance with the magnetic force. Additionally, magnetic hNFs have practical applications for the degradation of both cationic and anionic dyes. Nevertheless, magnetic hNFs can be used for remediating pollution and water disinfection to solve environmental issues.

Experimental section

Materials. Copper(II) sulfate pentahydrate ($CuSO_4 \cdot 5H_2O$), gallic acid, Iron(III) acetylacetonate ($Fe(acac)_3$) (97%), 1,6-hexanediamine (98%), ethylene glycol, sodium acetate, hydrogen peroxide (H_2O_2, 25% w/v), isopropyl alcohol (IPA), methylene blue (MB), congo red (CR) and phosphate buffer saline (PBS) tablets were purchased from Sigma Aldrich. *Escherichia coli* ATCC 25922, *Staphylococcus aureus* ATCC 25923, *Candida albicans* ATCC 10231 were obtained from Erciyes University, Faculty of Pharmacy and Pharmaceutical Microbiology research laboratory culture collection. All solutions were prepared with ultrapure water (resistance 18.2 MΩ). All chemicals were of analytical grade and used without further purification.

Synthesis of amine-functionalized Fe_3O_4 NPs. Amine-functionalized Fe_3O_4 NPs were prepared according to reported literature with slight modifications.[16] In the synthesis of NPs, $Fe(acac)_3$ (0,1 g), 1,6 hexanediamine (1.2 g), sodium acetate (1.3 g) was dispersed in ethylene glycol (10 mL) to form transparent solution. Subsequently, the mixture was transferred to a Teflon-lined hydrothermal synthesis autoclave and was heated at 200 °C for six hours. After incubation, the product was allowed to cool down to 25 °C and washed with hot water and ethanol to remove unbound 1,6 hexanediamine. An external magnetic force collected the obtained product.

Synthesis of GANF. GANF was synthesized according to the reported approach.[7,42,43] Briefly, an aqueous solution of CuSO4 (120 mM, 66 μL) was added to 10 mL phosphate buffer saline (PBS) solution (10 mM, pH 7.2) containing 0.02 mg/mL gallic acid. After the incubation at 25 °C for 3 days, the mixture was centrifiged to collect the precipitates formed at the bottom. The obtained product was washed with deionized water and dried at 45 °C.

Synthesis of magnetic GANF (FeGANF). In the synthesis of FeGANF, different amounts of Fe_3O_4 NPs (10 mg and 20 mg) were added to 20 mL of gallic acid solution (1 mg mL^{-1}). The mixture was vigorously shaken with vortex for 1 h and then was added to PBS solution (10 mmol L^{-1}, pH 7.4). Subsequently, an aqueous solution of $CuSO_4$ (120 mmol L^{-1}) was added to the resulting mixture and incubated at 25 °C for three days without disturbing. The product was collected by external magnetic force and washed with water several times. Finally, synthesized magnetic nanoflowers were dried at 45 °C.

Peroxidase like activity of hNFs: Peroxidase-like activity of hNFs was studied by catalyzing the oxidation of guaiacol in the presence of H_2O_2. First, 1 mL of 45 mmol L^{-1} guaiacol and 1 mL of 22.5 mmol L^{-1} H_2O_2 were mixed in 1 mL buffer solution containing hNFs (1.5 mg). After incubation, the resulting mixture was centrifuged and color change of supernatant based on guaiacol oxidation was measured at 470 nm using UV-Vis spectrophotometer. PBS (10 mmol L^{-1}, pH 7), sodium acetate (10 mmol L^{-1}, pH 4) and Na_2CO_3/$NaHCO_3$ (10 mmol L^{-1}, pH 10) were used as buffer solutions for determining optimum conditions.

Dye degradation. MB and CR were chosen as typical dyes to investigate the degradation efficiency of hNFs. At first stock dye solutions (0.5 mg mL^{-1}) were prepared. Then 1 mL stock dye solutions were mixed with 1 mL H_2O_2 (22.5 mmol L^{-1}) and 1 mL hNFs (1.5 mg) using the buffer solutions described above. The reaction mixture was incubated at room temperature.

The hNFs were separated by centrifugation or magnetic force. The absorbance values of supernatant were measured at the characteristic absorption wavelength of each dye at an interval of 15 min. The following equation was used to calculate dye decolorization in Eq. 3.

$$\% \text{ Dye decolorization} : [(A_0\text{-}A_1)/A_0]^*100 \quad (3)$$

A_0: The absorbance value at the degradation time of 0 min. A_1: The absorbance value at a certain time.

To test the reusability of FeGANF-20, these were collected and washed with deionized water and then added to a new dye solution containing H_2O_2. This process was repeated eigth times to test the repeatability of hNFs.

Antimicrobial activity of hNFs. The antimicrobial activities of hNFs were performed against *E. coli* ATCC 25922, *S. aureus* ATCC 25923 and *C. albicans* ATCC 10231 using disk diffusion method. Bacteria cells were grown at 37 °C for 24 h in Mueller Hinton Agar (MHA) and fungi cells were cultured at 37 °C for 24 h in RPMI. The 6 mm diameter sterile discs were impregnated with 25 μg mL^{-1} of each sample and incubated at 37 °C for 24 h or 48 h for bacteria or fungi, respectively. After incubation period, the diameters (mm) of inhibition zones were measured. The minimal inhibitory concentration (MIC) values were determined by the broth microdilution method from serial dilutions of GA and hNFs (1000 to 50 μg mL^{-1}) in MH broth (MHB) for bacteria and RPMI medium for *C. albicans*. The concentrations of microorganism were 1×10^8 CFU mL^{-1} at 0.5 McFarland standard turbidity. GA, hNFs and bacterial and fungi cell solutions were separately mixed in 96-well microplates and incubated at 37 °C for 24 h for bacteria and 48 h for *C. albicans*. Plates without any GA or hNFs were used as negative control.

Acknowledgements

We appreciate Erciyes University Technology Research and Implementation Center for assistance with SEM operation. This work was supported by a grant from the Erciyes University Scientific Research Office (TDK-2021-11004). M. H.C and O. L.F. acknowledge Fundação de Apoio à Pesquisa do Distrito Federal (FAPDF), Coordenação de Aperfeiçoamento de Pessoal de Nível Superior (CAPES), Conselho Nacional de Desenvolvimento e Tecnológico (CNPq) and Fundação de Apoio ao Desenvolvimento do Ensino, Ciência e Tecnologia do Estado de Mato Grosso do Sul (FUNDECT), Brazil.

Conflict of Interest

The authors declare that they have no known competing financial interests or personal relationships that could have appeared to influence the work reported in this paper.

Data Availability Statement

Supporting information includes degradation performance of MB in the presence of different concentration of IPA.

Keywords: Antimicrobial activity · Dye degradation · Hybrid nanoflowers · Magnetic nanoparticles · Peroxidase like activity

[1] M. Faustini, L. Nicole, E. Ruiz-Hitzky, C. Sanchez, *Adv. Funct. Mater.* **2018**, *28*, 1704158.
[2] J. Ge, J. Lei, R. N. Zare, *Nat. Nanotechnol.* **2012**, *7*, 428.
[3] Z. F. Wu, Z. Wang, Y. Zhang, Y. L. Ma, C. Y. He, H. Li, L. Chen, Q. S. Huo, Z. Q. Li, *Sci. Rep.* **2016**, *1*, 22412.
[4] C. Celik, N. Ildiz, I. Ocsoy, *Sci. Rep.* **2020**, *10*, 2903.
[5] A. Baldemir, N. B. Kose, N. Ildiz, S. Ilgun, S. Yusufbeyoglu, V. Yilmaz, I. Ocsoy, *RSC Adv.* **2017**, *7*, 44303.
[6] J. Y. Sun, J. C. Ge, W. M. Liu, M. H. Lan, H. Y. Zhang, P. F. Wang, Y. M. Wang, Z. W. Niu, *Nanoscale* **2014**, *6*, 255.
[7] S. Dadi, C. Celik, I. Ocsoy, *Sci. Rep.* **2020**, *10*, 16765.
[8] J. Rong, T. Zhang, F. Qiu, Y. Zhu, *ACS Sustainable Chem. Eng.* **2017**, *5*, 4468.
[9] Z. Lin, Y. Xiao, Y. Q. Yin, W. L. Hu, W. Liu, H. H. Yang, *ACS Appl. Mater. Interfaces* **2014**, *6*, 10775.
[10] C. Altinkaynak, S. Tavlasoglu, R. Kalin, N. Sadeghian, H. Ozdemir, I. Ocsoy, N. Ozdemir, *Chemosphere* **2017**, *182*, 122.
[11] Z. Shu, H. Wu, H. Lin, T. Li, Y. Liu, F. Ye, X. Mu, X. Li, *Biochem. Eng. J.* **2016**, *115*, 56.
[12] W. Jo, R. J. Tayade, *J. Environ. Chem. Eng.* **2016**, *4*, 319–327.
[13] E. S. Baeissa, *J. Alloys Compd.* **2016**, *672*, 564–570.
[14] X. S. Rong, F. X. Qiu, J. Rong, X. L. Zhu, J. Yan, D. Y. Yang, *Mater. Lett.* **2016**, *164*, 127-−131.
[15] M. J. Lima, C. G. Silva, A. M. Silva, J. C. Lopes, M. M. Dias, J. L. Faria, *Chem. Eng. J.* **2017**, *310*, 342–351.
[16] Y. Li, X. Xu, C. Deng, P. Yang, X. Zhang, *J. Proteome Res.* **2007**, *6*, 3849–3855.
[17] L. Gao, J. Zhuang, L. Nie, J. Zhang, Y. Zhang, N. Gu, X. Yan, *Nat. Nanotechnol.* **2007**, *2*, 577–583.
[18] S. Wu, D. Guo, X. Xu, J. Pan, X. Niu, *Sens. Actuators, B* **2020**, *303*, 127225.
[19] Y. Y. Xu, M. Zhou, H. J. Geng, J. J. Hao, Q. Q. Ou, S. D. Qi, X. Chen, *Appl. Surf. Sci.* **2012**, *258*, 3897–3902.
[20] L. Wang, J. Bao, L. Wang, F. Zhang, Y. Li, *Chem.-Eur. J.* **2006**, *12*, 6341–6347.
[21] Y. Yu, X. Fei, J. Tian, L. Xu, X. Wang, Y. Wang, *Colloids Surf. B* **2015**, *130*, 299–304.
[22] Q. Wang, L. Jiao, H. Du, Y. Wang, H. Yuan, *J. Power Sources* **2014**, *245*, 101–106.
[23] D. Guo, Q. Huang, R. Zhao, W. Guo, K. Fan, Z. Han, D. Nie, *Food Control* **2023**, *146*, 109540.
[24] B. Maddah, A. Sabouri, M. Hasanzadeh, *J. Polym. Environ.* **2017**, *25*, 770–780.
[25] H. J. Cheon, M. D. Adhikari, M. Chung, T. D. Tran, J. Kim, M. I. Kim, *Adv. Healthcare Mater.* **2019**, *8*, 1801507.
[26] D. A. Nichela, A. M. Berkovic, M. R. Costante, M. P. Juliarena, F. S. G. Einschlag, *Chem. Eng. J.* **2013**, *228*, 1148.
[27] Z. Hashemi, Z. M. Mizwari, S. Mohammadi-Aghdam, S. Mortazavi-Derazkola, M. A. Ebrahimzadeh, *Arabian J. Chem.* **2022**, *15*, 103525.

[28] Z. Hashemi, M. Shirzadi-Ahodashti, S. Mortazavi-Derazkola, M. A. Ebrahimzadeh, *Inorg. Chem. Commun.* **2022**, *139*, 109320.
[29] M. Shirzadi-Ahodashti, Z. Hashemi, Y. Mortazavi, K. Khormali, S. Mortazavi-Derazkola, M. A. Ebrahimzadeh, *Colloids Surf., A* **2021**, *617*, 126383.
[30] J. Jiao, X. Xin, X. Wang, Z. Xie, C. Xia, W. Pand, *RSC Adv.* **2017**,*7*, 43474.
[31] L. Yuan, M. Q. Yang, Y. J. Xu, *Nanoscale* **2014**, *6*, 6335.
[32] S. Verma, B. T. Rao, J. Jayabalan, S. K. Rai, D. M. Phase, A. K. Srivastava, R. Kaul, *J. Environ. Chem. Eng.* **2019**, *7*, 103209.
[33] R. W. Jadhav, D. D. La, V. G. More, H. Tung Vo, D. A. Nguyen, D. L. Tran, S. V. Bhosale, *Sci. Rep.* **2020**, *10*, 1–8.
[34] S. Jain, A. Panigrahi, T. K. Sarma, *ACS Omega* **2019**, *4*, 13153-—13164.
[35] X. Liu, F. Wu, C. Au, G. Li, J. Cheng, Y. Ling, K. Liao, *React. Kinet., Mech. Catal.* **2020**, *130*, 1109-—1121.
[36] T. Wang, X. Bi, L. Wang, M. Liu, W. Y. William, Z. Zhu, N. Sui, *J. Colloid Interface Sci.* **2022**, *607*, 470–478.
[37] W. X. Wang, K. J. Xiao, L. Zhu, Y. R. Yin, Z. M. Wang, *RSC Adv.* **2017**, *7*, 21287.
[38] N. A. Zubir, C. Yacou, J. Motuzas, X. Zhang, X. S. Zhaoa, J. C. D. Costa, *Chem. Commun.* **2015**, *51*, 9291.
[39] M. A. Ebrahimzadeh, Z. Hashemi, M. Mohammadyan, M. Fakhar, S. Mortazavi-Derazkola, *Surf. Interfaces* **2021**, *23*, 100963.
[40] Z. Chen, Z. Wang, J. Ren, X. Qu, *Acc. Chem. Res.* **2018**, *51*, 789.
[41] J. Xi, G. Wei, L. An, Z. Xu, Z. Xu, L. Fan, L. Gao, *Nano Lett.* **2019**, *19*, 7645–7654.
[42] A. Demırbas, B. Karslı, S. Dadi, F. D. Koca, M. G. Halıcı, I. Ocsoy, *ChemistrySelect* **2022**, *7*, e202202715.
[43] S. G. Yilmaz, A. Demirbas, Z. Karaagac, S. Dadi, C. Celik, S. Yusufbeyoglu, N. Ildiz, A. K. Mandal, B. Cimen, I. Ocsoy, *J. Biotechnol.* **2022**, *343*, 96–101.

Submitted: February 2, 2023
Accepted: March 17, 2023